

行政院國家科學委員會補助專題研究計畫

成果報告

期中進度報告

(計畫名稱)

Study of terahertz generation processes in doped GaSe crystals

計畫類別： 個別型計畫 整合型計畫

計畫編號：NSC 96-2923-M-009-001-MY3

執行期間：96年8月01日至99年7月31日

計畫主持人：羅志偉

共同主持人：吳光雄、莊振益

計畫參與人員：古新安、朱韋臻

成果報告類型(依經費核定清單規定繳交)： 精簡報告 完整報告

本成果報告包括以下應繳交之附件：

赴國外出差或研習心得報告一份

赴大陸地區出差或研習心得報告一份

出席國際學術會議心得報告及發表之論文各一份

國際合作研究計畫國外研究報告書一份

處理方式：除產學合作研究計畫、提升產業技術及人才培育研究計畫、
列管計畫及下列情形者外，得立即公開查詢

涉及專利或其他智慧財產權， 一年 二年後可公開查詢

執行單位：交通大學 電子物理系

中 華 民 國 98 年 5 月 27 日

1. Contents:

1-1. Background

Recently, there is growing interest in fields using terahertz (THz) waves, or T-rays, for spectroscopy, imaging, communications, signal processing, and quantum information. The prospects of T-rays applications could be imaged by the lifelike cover picture of Rensselaer Magazine [1]. Why do they call it “Next Rays”? In the viewpoint of safety, the T-rays will not cause harmful photoionization in biological tissues due to their low photon energies (4 meV@ 1THz, one millions times weaker than an x-ray photon). Moreover, numerous organic molecules have rotational and vibrational transitions which lead to strong absorption and dispersion in the region from GHz to THz. These characteristics are specific to the targets and enable T-rays fingerprinting. So T-rays are the wave of the future. In the past decade, this previously hidden region of the electromagnetic spectrum has caught the imagination of scientists around the world.

Terahertz domain of electromagnetic radiation spectrum (approximately 15 μm – 10 mm or 0.03 – 20 THz) is located between mid IR and microwave range and remains comparatively low investigated. That is connected with technical and technological difficulties in creation of corresponded element base (radiating and detecting devices, lenses, filters etc.). On the other hand, terahertz radiation possesses a set of important for practical applications properties. For instance, it has higher penetrating power than optical radiation and allows more detailed imaging than microwaves. It can propagate through most of non-metallic and non-polar media. Many characteristic features of different substances lie in this range, for instance rotational and oscillating frequencies of molecules. On the base of THz radiation source it is possible to create a remote detector of explosive substances with high spatial resolution. Terahertz spectroscopy becomes an important tool of molecular biology, electrophysics, medicine etc.

Early research concentrated on the generation and detection of THz radiation. By present time one can get terahertz radiation by dipole antennas [2-4], from semiconductor surface [5], by gas lasers with optical pump [6], free-electron lasers [7], and quantum-cascade lasers [8]. All methods have their merits and deficiencies. It is possible to obtain broad-band radiation with microwave lamps, but it is not coherent, free-electron lasers allows to get radiation in wide range and with high output power, but they are not compact and expensive thus being not available for most of research laboratories.

A way to create relatively compact and not expensive coherent terahertz radiation source is nonlinear optical conversion in nonlinear crystals. By the moment the best results, in terms of tuning range and peak output powers are obtained on GaSe and ZnGeP₂ crystals [9, 10]. Tuning range of some thousands of micrometers and peak powers of some hundreds of watts were achieved. On the other hand the task of optimizing the crystal properties is real. GaSe possesses low mechanical properties, as it is layered and easy cleavable material,

which makes a task to grow long homogeneous crystal difficult and do not allow to produce optical surfaces at angles to optical axis, that is needed for optimization of some types of frequency converters. Also ZnGeP₂ has rather low transparency and refractive indices.

GaSe crystals have being grown since 1960s. Original technology of manufacturing was developed by lab the participant of the project. The crystals are commercially available and used by many research labs for IR and THz applications. It was shown that doping could improve mechanical and optical properties of the materials.

1-2 Goals

In this project, we planed to find conditions of growth of large homogeneous GaSe crystals with lower absorption in THz region and investigate the possibilities to enhance their characteristics in THz generation and frequency convert by doping. The efficiency of conversion and in turn the power of output radiation is limited by crystal properties such as optical transparency and homogeneity. Additionally, the second method to generate THz is employing of dipole antenna scheme. For enhancement of efficiency of such devices it is necessary to use materials with high resistance and carrier mobility. Electrical transport properties of GaSe can be considerably modified by doping and it looks reasonable to investigate dipole antennas based on doped crystals, which also should give information on their electronic properties. After getting the suitable nonlinear optical crystals for high power and widely tunable wavelength THz generation, we could study the ultrafast dynamics in some interesting materials such as high T_c superconductor, multiferroics manganites, magnetic semiconductors and semiconductor quantum dots etc..

Finally the task is to develop scientifically based and stable schemes to produce nonlinear optical single crystals with improved parameters for applications in the THz range.

1-3 Results and discussions

(1) In Russia:

The S-doped and Te-doped GaSe crystals have been grown by the way of modified two-temperature method (horizontal variant). The temperature-temporary conditions are as follows,

- Growth rate is within 0.5-1 mm/hour.
- Melt temperature is within 1010-1020 °C;
- Temperature gradient at the crystallization front is 10 degree/cm;

Specimens with thickness of 0.5 mm and 1.0 mm were made for investigation of physical properties and study of frequency conversion processes by exfoliation method from grown single crystal boules. A few millimetres to few centimetres sized specimens of mixed crystals were made by mechanical methods: diamond saw cut and mechanical

polishing, so as it fixing on a metal substrate with the aperture of 5-10 mm in diameter for preservation of specimen flatness, as shown in Fig. 1.

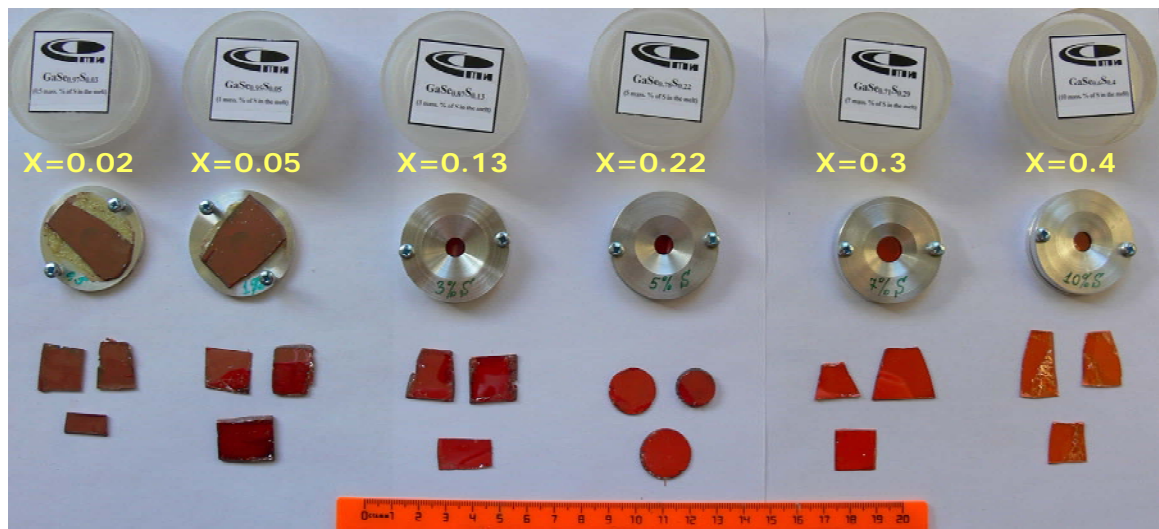


Fig. 1 External view of the samples, $\text{GaSe}_{1-x}\text{S}_x$.

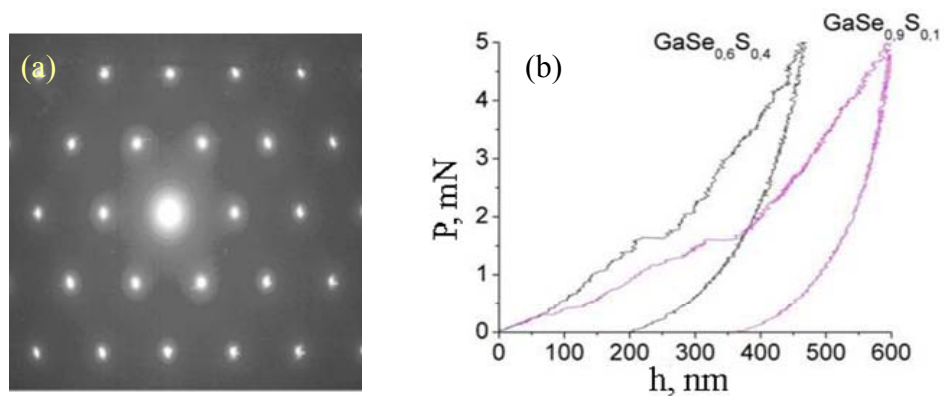


Fig. 2 (a) Electron diffraction pattern. (b) Loading diagrams for the surface parallel to the $\text{GaSe}_{1-x}\text{S}_x$ layers.

The crystallinity of S-doped GaSe crystals have been measured by the electron diffraction pattern which shown the hexagonal structure in ab -plane (see the Fig. 2(a)). Moreover, the strength of bonds between the layers increases with raising the content of sulfur as shown in Fig. 2(b). This means that the hardness of GaSe crystals effectively rises with doping.

(2) In Taiwan:

A THz time-domain spectroscopy (TDS) system with a focused beam at the position of a sample has been used in this study as shown in Fig. 3. The THz pulses, generated by femtosecond-laser-excited dipolelike antenna fabricated on semiconductor InP, were collimated by the off-axis paraboloidal mirror and focused on the sample by the other off-axis paraboloidal mirror. The spot size of the THz wave through the sample is about 4 mm in diameter which is smaller than the size of samples to increase the signal to noise ratio. The transmitted THz pulses were collected and focused on a (110)-oriented ZnTe crystal. The detection of THz wave using the free-space electro-optic sampling technique [11] was setup on a mode-locked Ti:sapphire laser operating at 800 nm (1.55 eV) with an 80 MHz train of 50 fs pulses. The entire setup was placed in an airtight enclosure purged with dry nitrogen and maintained at a relative humidity of < 2.0 % to avoid the strong absorption of water vapor in THz range.

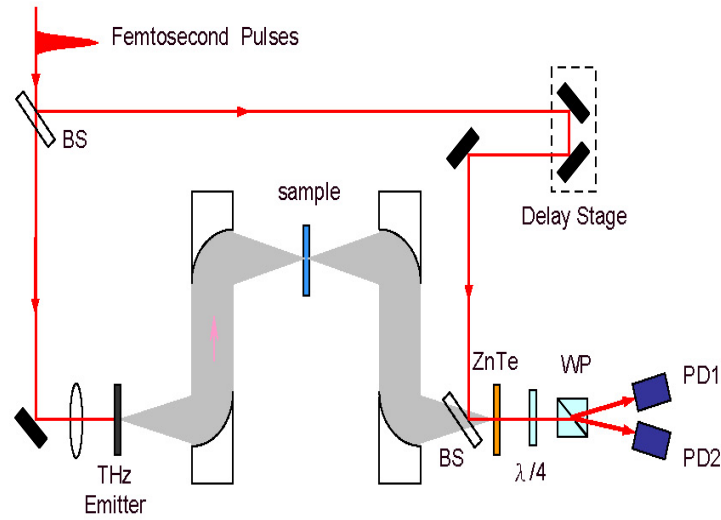


Fig. 3 Schematic of the THz-TDS. BS: Beam splitter. WP: Wollaston polarizer. DP1 and DP2: Photodiode 1 and photodiode 2, respectively.

The temporal profiles of the THz pulse transmitted through the samples and air are shown in Fig. 4(a). After through the $\text{GaSe}_{1-x}\text{S}_x$ crystals, the THz pulses do not only shrink in amplitude but also delay in time. The delay (Δt) from reference THz pulse (the thick line in Fig. 4(a)) is due to the thickness and the refractive index of $\text{GaSe}_{1-x}\text{S}_x$ crystals. From the measured delay time Δt , the group index of refraction is calculated by $n_g = 1 + c\Delta t/d$, where d is the thickness of samples, and c is the speed of light in vacuum. For the thinnest crystals ($\text{GaSe}_{0.95}\text{S}_{0.05}$) with 240 μm , the $n_g = 3.1$ is consistent with the measured values in the range of 0.2-1.5 THz at room temperature (see Fig. 5). In this study, the propagation direction of the incident THz beam with horizontal polarization is parallel with the optical axis (normal to the surface). Thus the refractive index measured in this geometry is the ordinary index, n_o .

Figure 4(b) shows the frequency spectra in THz range which are directly transferred from the THz signal in time domain by Fourier Transform method. In order to eliminate the modulation in the frequency spectra, the data analysis was only performed on the main pulse. The refractive index at various frequencies (ν) is determined by the phase difference as $n(\nu)=1+c\Delta\theta/2\pi\nu d$, and the absorption coefficient is calculated as $\alpha(\nu)=-\ln[\eta \cdot P_s(\nu, d)/P_r(\nu, d)]/d$ [12], where η is a correcting factor related to the reflection losses at the two crystal/air interfaces. $P_s(\nu, d)$ and $P_r(\nu, d)$ are the measured transmittances for sample and reference (without sample), respectively. Above analyses enabled the quite accurate determination of the refractive index $n(\nu)$ and power absorption $\alpha(\nu)$ for the $\text{GaSe}_{1-x}\text{S}_x$ crystals as shown in Fig. 5 and Fig. 6, respectively.

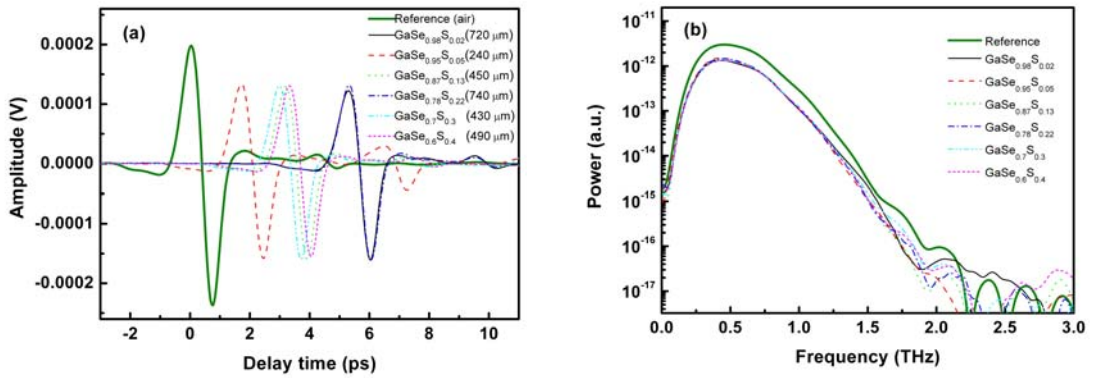


Fig. 4 (a) Temporal profiles of the THz pulse transmitted through $\text{GaSe}_{1-x}\text{S}_x$ crystals and air (thick-solid line). (b) The power spectra of the THz pulse transmitted through $\text{GaSe}_{1-x}\text{S}_x$ crystals and air (thick-solid line).

Although the refractive index $n(\nu)$ of $\text{GaSe}_{1-x}\text{S}_x$ crystals is almost constant in THz range, the refractive index is strongly doping-dependent, i.e. $n(\nu)$ gradually decreases with increasing x in heavy S-doping region ($x > 0.22$). In 1995, Vodopyanov *et al.* [13] successfully fitted the refractive index of GaSe in 0.65-18 μm by the following dispersion equation:

$$n_{0,\text{GaSe}}^2 = A + \frac{B}{\lambda^2} + \frac{C}{\lambda^4} + \frac{D}{\lambda^6} + \frac{E\lambda^2}{\lambda^2 - F} \quad (1)$$

where λ is in microns and the values for the coefficients $A = 7.4430$, $B = 0.4050$, $C = 0.0186$, $D = 0.0061$, $E = 3.1485$, $F = 2194$. We further apply the Eq. (1) to THz range and plot with thick-solid line in Fig. 5, which is consistent with the results in Ref. [12]. Obviously, all of the refractive indexes of S-doped GaSe crystals are smaller than the values from Eq. (1). This may be due to the β -GaS phase with lower refractive index. According to the studies in the dispersion properties of the $\text{GaSe}_{1-x}\text{S}_x$ nonlinear solid solution crystals in Ref. [14], the refractive index of $\text{GaSe}_{1-x}\text{S}_x$ crystal in THz range could be estimated by

$$n_{0,\text{GaSe}_{1-x}\text{S}_x}^2 = (1-x) \cdot n_{0,\text{GaSe}}^2 + x \cdot n_{0,\text{GaS}}^2 \quad (2)$$

where

$$n_{0,\text{GaS}}^2 = A/\lambda^4 + B/\lambda^2 + C + D\lambda^2 + E\lambda^4 \quad (3)$$

By fitting the experimental data of $\text{GaSe}_{0.6}\text{S}_{0.4}$ in Fig. 5 with the Eq. (2), the coefficients in Eq. (3) are $A = -3.4777 \times 10^7$, $B = -2984$, $C = 6.7440$, $D = 3.3382 \times 10^{-7}$, $E = -8.6732 \times 10^{-14}$. It is worthwhile emphasizing that the dash-dotted and dash-dot-dotted lines plotted by Eq. (2) match, respectively, with the experimental data of $\text{GaSe}_{0.78}\text{S}_{0.22}$ and $\text{GaSe}_{0.7}\text{S}_{0.3}$ quite well. However, the refractive index of slightly S-doped GaSe crystals ($x \leq 0.13$) cannot be expressed by the Eq. (2). This implies that the β -GaS phase certainly form in the heavy S-doped GaSe crystals ($x \geq 0.22$).

Moreover, some absorption resonance structures in the power absorption spectra (marked by the arrows in the inset of Fig. 6) are attributed to the second-order phonon modes which are the frequency differences between combinations of acoustical and optical phonons [15]. As listed in Table 1, three absorption peaks, 0.232 THz (7.7 cm^{-1}), 0.585 THz (19.5 cm^{-1}), 1.025 THz (34.2 cm^{-1}), were clearly observed in the power absorption spectrum of $\text{GaSe}_{0.98}\text{S}_{0.02}$ crystal. While increasing the content of S in $\text{GaSe}_{1-x}\text{S}_x$ crystals, the positions of the absorption peaks shift to higher frequency or larger wave number, e.g. $\text{GaSe}_{0.95}\text{S}_{0.05}$ in Table 1. However, these absorption peaks would be smeared in heavy S-doped GaSe samples as shown in Fig. 6. For the cases of $\text{GaSe}_{0.78}\text{S}_{0.22}$, $\text{GaSe}_{0.7}\text{S}_{0.3}$, and $\text{GaSe}_{0.6}\text{S}_{0.4}$, no significant structures were observed in the power absorption spectra. By the Raman experiments in Ref. 16, Hayek *et al.* showed that the phonon spectra of $\text{GaSe}_x\text{S}_{1-x}$ are strongly S-doping-dependent. With increasing the content of S in GaSe crystals, namely, the phonon peaks were shifted to higher frequency or disappear gradually; meanwhile, some new phonon peaks were created. Consequently, the absorption peaks in the cases of $\text{GaSe}_{0.98}\text{S}_{0.02}$ and $\text{GaSe}_{0.95}\text{S}_{0.05}$ clearly disappear for $x > 0.05$ due to the emergence of the β -GaS phase in $\text{GaSe}_{1-x}\text{S}_x$. These results disclose that the optical properties of the heavy S-doped GaSe crystals ($\text{GaSe}_{1-x}\text{S}_x$, $x > 0.13$) in THz range are dominated by the β -GaS phase.

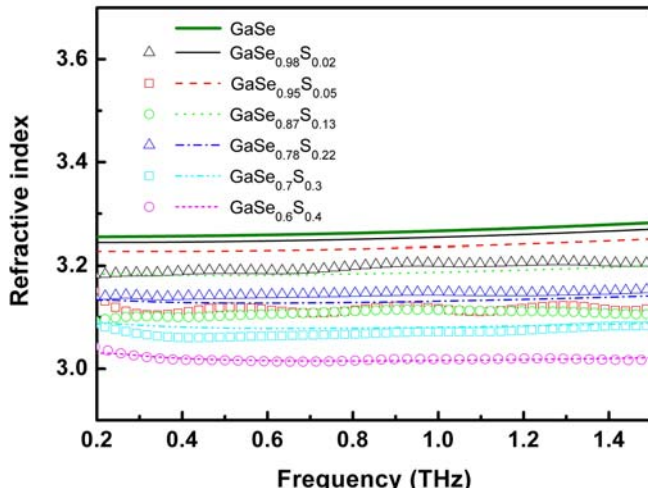


Fig. 5 Refractive index of the $\text{GaSe}_{1-x}\text{S}_x$ crystals in THz range (symbolic points). All of the lines are drawn by the Eq. (2).

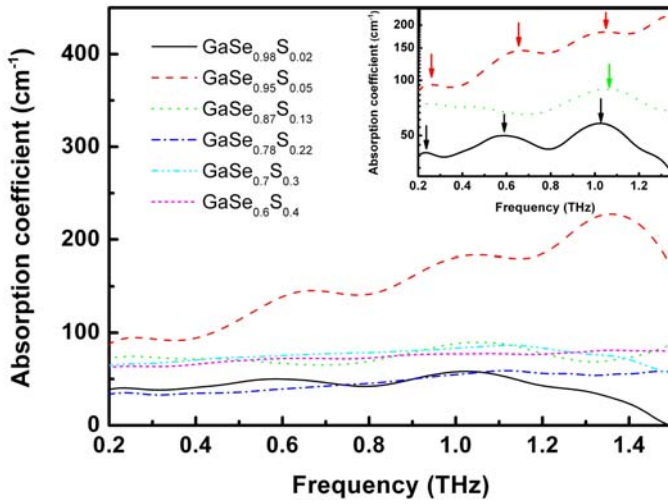


Fig. 6 Power absorption spectra of the $\text{GaSe}_{1-x}\text{S}_x$ crystals in THz range. The inset shows the power absorption spectra of the slightly S-doped GaSe crystals in logarithm scale.

Table 1. Assignment of the different combinations of phonon modes in $\text{GaSe}_{1-x}\text{S}_x$ crystals.

Samples	TDS		Second-order phonon modes	
	THz	(cm^{-1})	Combination assignment in symmetry species	Calculated from modes in Ref. 24 (cm^{-1})
$\text{GaSe}_{0.98}\text{S}_{0.02}$	0.232	(7.7)	$A'_1 - A'_1$	$142.6 - 134.0 = 8.6$
	0.585	(19.5)	$A''_2(\text{TO}) - E'(\text{TO})$	$233.4 - 214.0 = 19.4$
	1.025	(34.2)	$A''_2(\text{LO}) - E'(\text{TO})$	$247.6 - 214.0 = 33.6$
$\text{GaSe}_{0.95}\text{S}_{0.05}$	0.262	(8.7)	$A'_1 - A'_1$	$143.0 - 133.2 = 9.8$
	0.665	(22.2)	$A''_2(\text{TO}) - E'(\text{TO})$	$233.0 - 212.6 = 20.4$
	1.047	(34.9)	$A''_2(\text{LO}) - E'(\text{TO})$	$248.0 - 212.6 = 35.4$
$\text{GaSe}_{0.87}\text{S}_{0.13}$	1.082	(36.1)	$2A' - E_{2g}^1$	$316.3 - 277.8 = 38.5$

For THz measurement, an interferometric system was established as the Fig. 7.

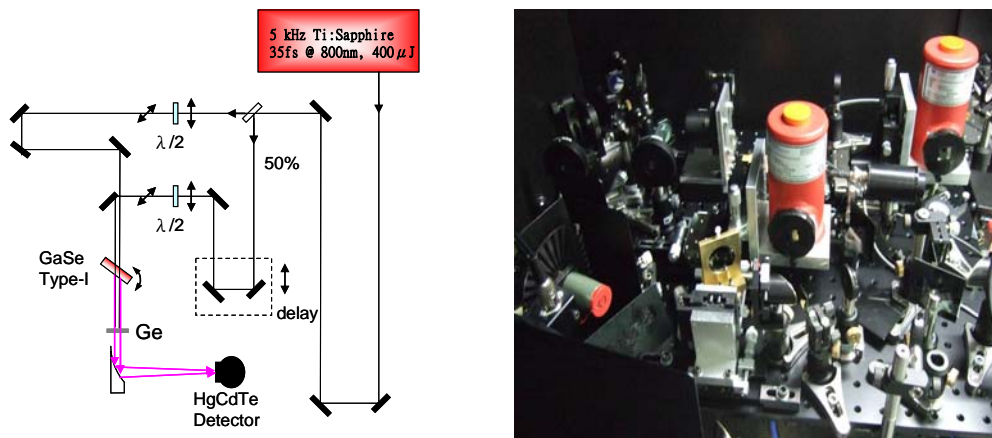


Fig. 7 Schematic of the THz interferometric system.

The THz frequency could be changed by adjusting the incident angle of NIR laser pulses. Fig. 8 shows the electric waveform of THz radiation at various incident angles. After Fourier transform, the angle dependence of THz frequency is clearly shown in Fig. 9(a). The maximum radiated power of THz is around 50° as shown in Fig. 9(b).

Moreover, it is worthwhile mentioning that the phase matching angle of GaSe with slightly S-doped could be extended to zero degree for THz generation as shown in Fig. 10.

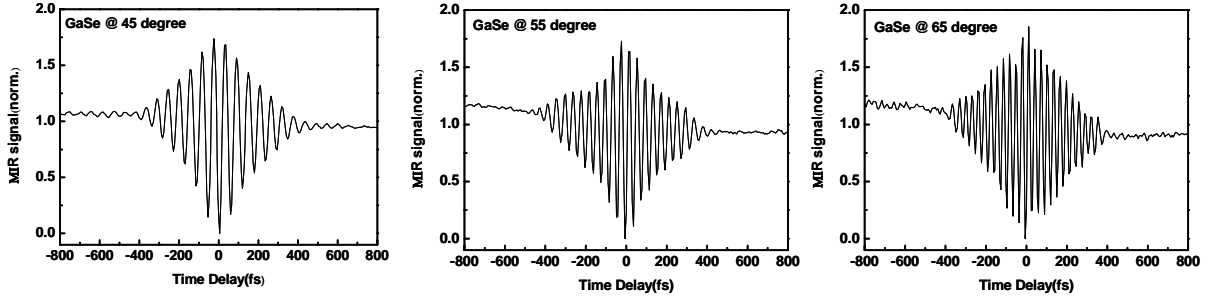


Fig. 8 The electric field of THz radiation in time domain.

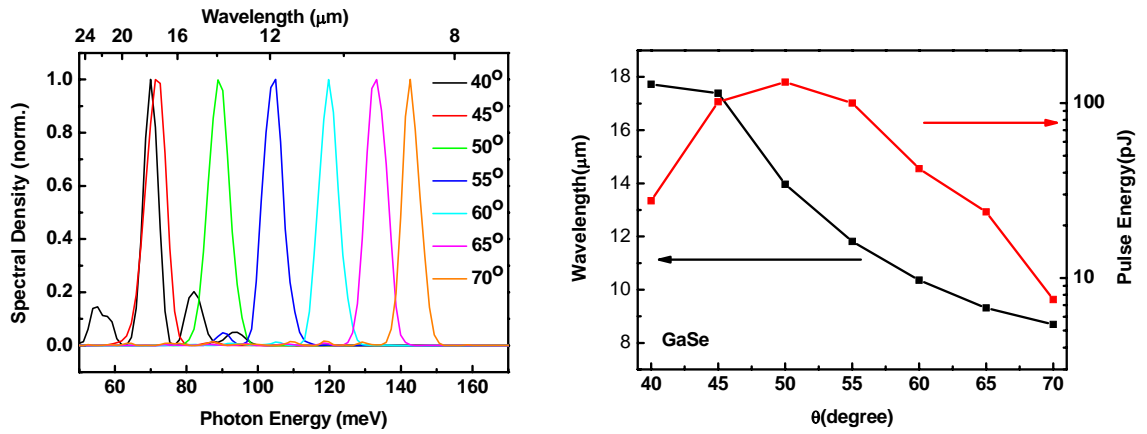


Fig. 9 (a) The Fourier Transform spectrum of THz waveform in Fig. 8. (b) The wavelength and output power as a function of incident angle.

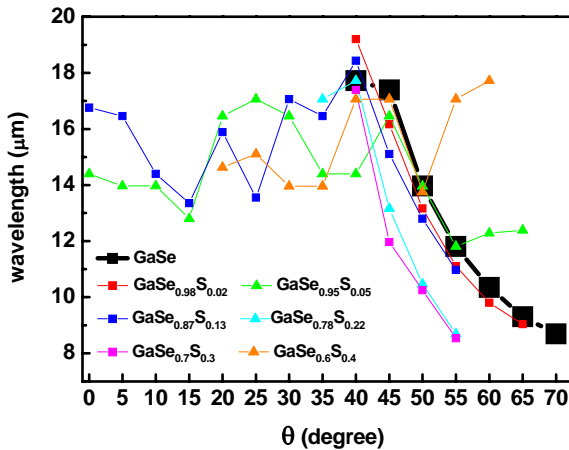


Fig. 10 The wavelength of THz radiation as a function of incident angle for various S-doping in GaSe crystals.

2. References:

- [1] The cover picture of Rensselear Magazine, <http://www.rpi.edu/change/zhang.html>.
- [2] D. H. Auston, Appl. Phys. Lett. **26**, 101 (1975).
- [3] A. G. Davies *et al.*, Phys. Med. Biol. **47**, 3679 (2002).
- [4] M. Tani *et al.*, Meas. Sci. Technol. **13**, 1739 (2002).
- [5] X.-C. Zhang *et al.*, Appl. Phys. Lett. **56**, 1011 (1990).
- [6] F. Klappenberger *et al.*, Int. J. of Infrar. and Millim. Waves **24**, 1405 (2003).
- [7] G. L. Carr *et al.*, Nature **420**, 153 (2002).
- [8] Ruedeger Koehler *et al.*, Nature **417**, 156 (2002).
- [9] W. Shi *et al.*, Appl. Phys. Lett. **84**, 1635 (2004).
- [10] W. Shi *et al.*, Opt. Commun. **233**, 183 (2004).
- [11] Q. Wu *et al.*, Appl. Phys. Lett. **67**, 3523-3525 (1995).
- [12] B. L. Yu *et al.*, Appl. Phys. Lett. **87**, 182104-1-182104-3 (2005).
- [13] K. L. Vodopyanov *et al.*, Optics Comm. **118**, 375-378 (1995).
- [14] S. A. Ku *et al.*, Russ. Phys. J. **51**, 1083-1089 (2008).
- [15] H. Yoshida *et al.*, Phys. Stat. Sol. (B) **59**, 655-666 (1973).
- [16] M. Hayek *et al.*, Phys. Rev. B **8**, 2772-2779 (1973).

Publication list :

1. **C. W. Luo**, Y. Q. Yang, I. T. Mak, Y. H. Chang, K. H. Wu and T. Kobayashi, 2008 February, *A widely tunable dual-wavelength CW Ti:sapphire laser with collinear output*, Opt. Express **16**, 3305 ~ 3309.
2. S. A. Ku, **C. W. Luo**, H. L. Lio, K. H. Wu, J. Y. Juang, A. I. Potekaev, O. P. Tolbanov, S. Yu. Sarkisov, Yu. M. Andreev, and G. V. Lanskii, “*Optical properties of nonlinear solid solution GaSe_{1-x}S_x (0 < x ≤ 0.4) crystals*”, Russ. Phys. J. **51**, 1083-1089 (2008).
3. **C. W. Luo**, S. A. Ku, W. C. Chu, S. Yu. Sarkisov, and Yu. M. Andreev “*The optical properties of sulfur-doped GaSe crystals in terahertz frequency range*”, submitted to Opt. Express (2009).

3. Self-evaluation:

In this Taiwan-Russia Research Cooperation project, the researchers in Russia have been prepared the various S-doped and Te-doped GaSe crystals last year and this year, respectively. All of the specimens have been delivered to Taiwan. After received the specimens from Russia, we immediately measured the transmissivity of all crystals in Far-IR and Mid-IR region by Fourier Transform Infrared Spectroscopy (FTIR). We found some interesting results in THz-TDS measurements which have been submitted to Optics Express. Moreover, we have successfully generated THz radiation from these GaSe:S and GaSe:Te crystals. There are some surprising results which are that the THz could be generated at small phase matching angle even at zero degree for slightly S-doped GaSe crystals. We are studying the mechanism of this phenomenon.

OPTICAL PROPERTIES OF NONLINEAR SOLID SOLUTION

GaSe_{1-x}S_x (0 < x ≤ 0.4) CRYSTALS

S.-A. Ku,¹ C.-W. Luo,¹ H.-L. Lio,² K.-H. Wu,¹
 J.-Y. Juang,¹ A. I. Potekaev,³ O. P. Tolbanov,³
 S. Yu. Sarkisov,³ Yu. M. Andreev,⁴ and G. V. Lanskiĭ⁴

UDC 621.378.325

Transmission spectra and phase matching conditions for second harmonic generation in GaSe_{1-x}S_x (0 < x ≤ 0.4) solid solution crystals are experimentally investigated. An algorithm is suggested and dispersion equations are derived that allow the phase matching angles describing best the available experimental data to be estimated as a function of the mixing ratio x.

INTRODUCTION

Nonlinear layered structure ϵ -GaSe crystals of $\bar{6}m2$ point group symmetry have not found practical application in spite of a wide variety of attractive physical properties because of almost zero hardness in Mohs scale and easy cleavage. Low mechanical properties have made their mechanical treatment impossible, and working elements can be used only under laboratory conditions due to low exploitation characteristics. Moreover, cleavage defects mask their high natural nonlinear properties, decrease their damage threshold, and cause the occurrence of internal optical damages. Investigations performed previously have demonstrated the advantages of the layered nonlinear solid solution crystals (NSSC) grown according to the chemical formula GaSe : GaS \rightarrow GaSe_{1-x}S_x ($x \leq 0.412$) over the initial ϵ -GaSe crystals. Variations of the mixing ratio x in the stage of technological growth processes allowed the researchers to control a number of physical properties of the GaSe_{1-x}S_x NSSC and, as a consequence, the phase matching (PM) condition for parametric frequency conversion. Elimination of the cleavage defects caused the hardness to increase, and the GaSe_{1-x}S_x NSSC suitable for mechanical treatment and polishing were synthesized. The internal damages disappeared, the thermal conductivity in the direction perpendicular to the growth layers increased, and the damage threshold increased. As a result, the modification of physical properties increased the efficiency of frequency converters based on the GaSe_{1-x}S_x NSSC several times compared to the frequency converters based on the ϵ -GaSe crystals and even on the ZnGeP₂ crystals [1–7], the so-called “mid-IR nonlinear crystal standard” [8]. This modification of properties can also significantly improve the exploitation characteristics of the frequency converters.

On the other hand, despite the obvious prospects for practical application of the GaSe_{1-x}S_x NSSC, equations suitable for estimating their dispersion properties as functions of the mixing ratio x (the spectral dependence of the refractive index $n_{o,e}$ for ordinary and extraordinary waves) have yet to be derived. The well-known dispersion equations for the GaSe_{1-x}S_x ($x = 0, 0.2, 0.4, 0.8, \text{ and } 1.0$) NSSC [1] are insufficient for the derivation of the dispersion equations with coefficients being continuous functions of the mixing ratio x and adequately describing the PM conditions. The data on the dispersion properties of the initial ϵ -GaSe crystal available from the literature [9] differ significantly. Moreover, the literature data [1, 10, 11] contain only a very limited volume of information on the dispersion properties of the second GaS initial crystal. The GaS crystals have β -polytype structure [12]; therefore, the well-known expression [13]

¹National Chiao Tung University, Hsinchu, Taiwan; ²National Taiwan Normal University, Taipei, Taiwan; ³V. D. Kuznetsov Siberian Physical-Technical Institute of Tomsk State University, Tomsk, Russia; ⁴Institute of Monitoring of Climatic and Ecological Systems of the Siberian Branch of the Russian Academy of Sciences, Tomsk, Russia, e-mail: tolbanov@rid.tom.ru. Translated from *Izvestiya Vysshikh Uchebnykh Zavedenii, Fizika*, No. 10, pp. 80–85, October, 2008. Original article submitted June 19, 2008.

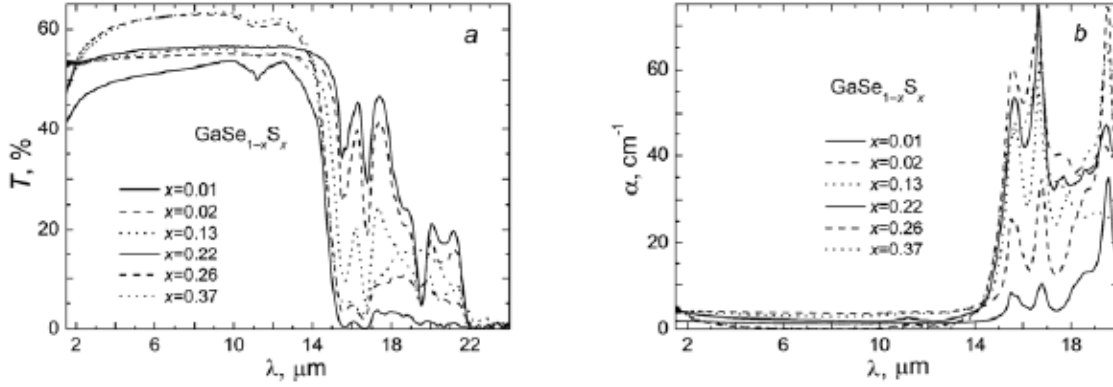


Fig. 1. Transmission spectra (a) and absorption coefficients (b) of $\text{GaSe}_{1-x}\text{S}_x$ crystals in the mid-IR range. The crystal structures are indicated in the insert.

$$n_{0,e}^2[\text{NSSC}] = (1-x) \cdot n_{0,e}^2[1^{\text{st}} \text{ crystal}] + xn_{0,e}^2[2^{\text{nd}} \text{ crystal}] \quad (1)$$

cannot be used to estimate the dispersion properties of the $\text{GaSe}_{1-x}\text{S}_x$ NSSC without additional investigations. The matter is that expression (1) is applicable to estimation of the dispersion properties of the NSSC synthesized from initial crystals with identical crystal structures, and the $\text{GaSe}_{1-x}\text{S}_x$ NSSC, by analogy with the GaSe and GaS crystals, can have one of four polymorphic structures: centrally asymmetrical ϵ -, δ -, or γ -polytype or centrally symmetrical β -polytype structure belonging to the same point symmetry group. Moreover, the polytype of the grown $\text{GaSe}_{1-x}\text{S}_x$ NSSC is transformed when x changes, and transition from one polytype to another occurs at unambiguously uncertain x values depending on the growth technology. The natural $\text{GaSe}_{1-x}\text{S}_x$ NSSC samples frequently contain a mixture of crystals of various polytypes, and their structure and composition must be controlled in the entire volume of the samples involved in the process of frequency conversion. Since this can be made only by destructive methods, at present adequate selection of $\text{GaSe}_{1-x}\text{S}_x$ NSSC and manufacture of specimens are impossible for concrete types of the frequency converters.

The problem can be solved by proposing an algorithm for nondestructive selection of the $\text{GaSe}_{1-x}\text{S}_x$ NSSC suitable for application in nonlinear optical devices and by developing analytical expressions characterizing the dispersion properties as continuous functions of the mixing ratio x . Exactly this is the purpose of the present work.

1. EXPERIMENTAL INVESTIGATIONS

We investigated the $\text{GaSe}_{1-x}\text{S}_x$ NSSC grown by the Bridgeman method at the Siberian Physical-Technical Institute of Tomsk State University (SPTI TSU), Tomsk, and Ametist Federal State Unitary Enterprise, Krasnodar, Russia [3, 5]. Crystal samples with thicknesses of 0.5–2 mm were prepared by cleaving without additional treatment. The crystal structure of external layers of the samples was identified with an x-ray diffractometer as ϵ -polytype of $\bar{6}m2$ group symmetry. The chemical composition of the surface layers to depths of 50 Å was investigated by the method of x-ray electron emission microanalysis using a LEO-1430 electron microscope. The most probable values $x = 0.01, 0.02, 0.09, 0.13, 0.18, 0.22, 0.26, 0.29, 0.37,$ and 0.4 were found for local surface points of the samples 100 μm in diameter. Three samples of the pure ($x = 0$) GaSe crystal were also investigated. For most crystals, the gallium content exceeded its nominal structure by 1–2%.

As an example of optical properties, Fig. 1 shows transmission spectra of six examined $\text{GaSe}_{1-x}\text{S}_x$ NSSC samples with mixing ratios of the charge composition indicated in the parentheses: $\text{GaSe}_{0.99}\text{S}_{0.01}$ ($x = 0.02$ or 0.5 mass%

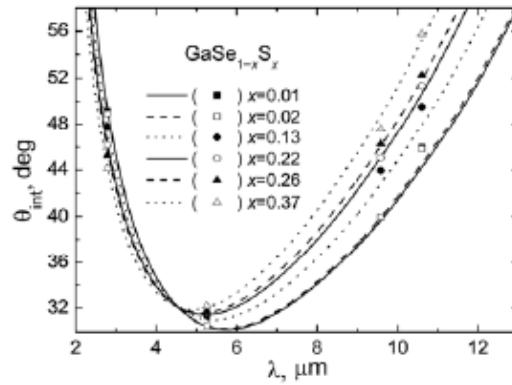


Fig. 2. Internal PM conditions for second harmonic generation with wavelengths of 2.79, 9.58, and 10.6 μm as functions of the mixing ratio x . Crystal types and corresponding mixing ratios are indicated in the insert.

for the initial charge and sample thickness of 0.75 mm, $\text{GaSe}_{0.98}\text{S}_{0.02}$ (0.05 or 1 mass% and 0.35 mm), $\text{GaSe}_{0.87}\text{S}_{0.13}$ (0.13 or 3 mass% and 0.40 mm), $\text{GaSe}_{0.78}\text{S}_{0.22}$ (0.22 or 5 mass% and 0.90 mm), $\text{GaSe}_{0.74}\text{S}_{0.26}$ (0.29 or 7 mass% and 0.50 mm), and $\text{GaSe}_{0.63}\text{S}_{0.37}$ (0.40 or 10 mass% and 0.55 mm).

We note that the sulfur content in most cases was much less than its nominal content in the charge. The transmission spectra were measured with wavelength resolution of 0.25 cm^{-1} with the help of a Bruker IFS 66v/S Fourier spectrophotometer. The absorption coefficient spectra calculated in the maximum transparency range (Fig. 1b) are qualitative in character because of small thickness of the examined NSSC samples.

Optical installations for second harmonic generation (SHG) of nanosecond Er^{3+} : YSGG laser (2.79 μm) and pulse periodic sealed-off CO_2 laser (generating at 9.58 and 10.6 μm) had conventional types and their composition was almost the same as in [7]. To interpret better the PM diagrams (see Fig. 2 in [7]), a pulse-periodic tunable CO_2 laser generating at the $9 \rightarrow 8(14)$ emission line at 5.25 μm with peak power up to 500 W and pulse duration of $\sim 1\ \mu\text{s}$ was also used in the present work. This allowed us to determine the PM angles in the vicinity of minima in the PM diagrams. Fine angular tuning of nonlinear crystals to the PM direction was performed with the help of an RCA100 positioning stage of Zolix Instruments Co., China, driven by a computer-controlled step motor providing positioning accuracy of $4.5''$. The total error in measuring the PM angle was determined by local deviations of the crystal surface from the plane and an air gap in the positioning stage; it was minimized by stage rotation in one direction. Deviations of the input surface from the plane had technological origin and also appeared as a result of sample preparation for investigations as well as during sample exploitation. This source of errors was minimized by means of control over the linearity of displacement of the reference helium-neon-laser beam on a screen placed at a distance of 2 m from the crystal. This procedure was performed simultaneously with tuning to the PM direction. The above-indicated measures allowed us to reduce the total error in measuring the PM angles to a satisfactory level of about $\pm 10'$. Figure 2 shows the measured PM conditions for second harmonic generation of Er^{3+} : YSGG (2.79 μm), CO (5.25 μm), and CO_2 lasers (9.2 and 10.6 μm).

2. ANALYSIS OF RESULTS OF INVESTIGATIONS

In Fig. 1, in addition to the shift of the long-wavelength end of the absorption spectrum for the $\text{GaSe}_{1-x}\text{S}_x$ NSSC toward shorter wavelengths, an absorption peak previously observed in [7] for crystal No. 9 can be seen around 11.25 μm . The presence of a short-wavelength absorption shoulder can also be seen for crystals with high mixing ratios. It was previously recorded in [2] (see Fig. 1) and in [7] for crystals Nos. 9 and 10 (see Fig. 3). Inclusions of spherical gallium particles of micron and submicron sizes were detected by the method of electron microscopy for crystals with

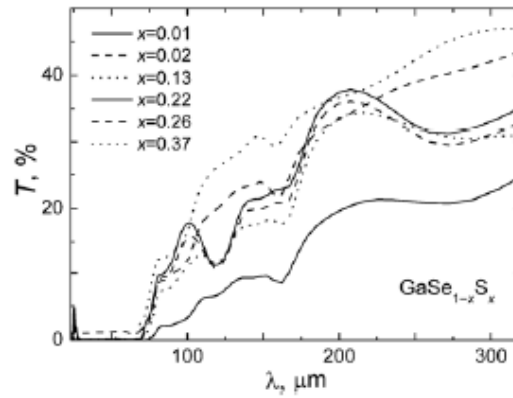


Fig. 3. Transmission spectrum of the $\text{GaSe}_{1-x}\text{S}_x$ NSSC in the terahertz range. The NSSC structure is specified in the insert.

short-wavelength absorption shoulder. This is in good agreement with the excess of the gallium content. A nature of the absorption peak around $11.25 \mu\text{m}$ has not yet been identified; it seems most likely that this peak is caused by the phonon absorption of one of the selenium compounds with excess content of gallium and deficient sulfur content to that in the charge.

In spite of the presence of the additional absorption peak and the absorption shoulder, the absorption spectra of all examined $\text{GaSe}_{1-x}\text{S}_x$ NSSC with $0.4 \geq x \geq 0.22$ are smoothed noticeably in the terahertz range; for high-quality samples, a decrease in optical losses in comparison to those in pure GaSe crystals and NSSC with small mixing ratio can be expected (Fig. 3). The transmission spectrum was measured with a home-made spectrophotometer that operated in the terahertz range of the spectrum with resolution of $1.12 \mu\text{m}$. We consider that the absorption spectrum is smoothed due to a decreased intensity of phonon absorption peaks caused by the presence of selenium in the crystal structure. Several remaining absorption peaks, for example, the peak around $165 \mu\text{m}$, are caused by the water vapor absorption.

An analysis of the data shown in Fig. 2 allowed us to conclude that the dependence of the PM conditions of second harmonic generation in the $\text{GaSe}_{1-x}\text{S}_x$ NSSC, as a kind of parametrical frequency conversion process, is linear or quasi-linear process. The linear dependence indicates identity of the $\text{GaSe}_{1-x}\text{S}_x$ ($x \leq 0.4$) NSSC crystal structure to ϵ -GaSe structure or, at least, centrally asymmetrical structure and the insignificant difference between the PM conditions in different asymmetrical-structure polytypes. The coincidence degree of the PM conditions to this linear dependence can serve as means for control of asymmetric structure and homogeneity of NSSC composition in the entire thickness. The dependence itself can be used to develop the dispersion equations as continuous functions of the mixing ratio $x \leq 0.4$. We note that the deviation of the PM angles from the linear dependence in Fig. 2 exceeds significantly a measurement error of $\pm 10'$ and is more likely statistical in character. It can be caused by the presence of variations of the mixing ratio in the volume of the examined NSSC. This is being checked now by the destructive chemical method that yields the sulfur content averaged over the NSSC volume. A possible reason for this difference can also be the presence of internal NSSC inhomogeneities caused by technological reasons.

3. DISPERSION EQUATIONS FOR THE $\text{GaSe}_{1-x}\text{S}_x$ ($x \leq 0.4$) SOLID SOLUTION CRYSTALS

The following algorithm was suggested to develop the equations describing the dispersion properties of the $\text{GaSe}_{1-x}\text{S}_x$ ($x \leq 0.4$) solid solution crystals in the mid-IR range. From the estimated PM angles calculated using all known dispersion equations for the ϵ -GaSe crystals [9], it was established that the available experimental results on second harmonic generation are best described by the following dispersion equations:

$$n_{0,e}^2 = A_{0,e} + B_{0,e}/\lambda^2 + C_{0,e}/\lambda^4 + D_{0,e}/\lambda^6 + E_{0,e}\lambda^2/(\lambda^2 - F_{0,e}) \quad (2)$$

with the coefficients $A_0 = 7.443$, $B_0 = 0.4050$, $C_0 = 0.0186$, $D_0 = 0.0061$, $E_0 = 3.1485$, and $F_0 = 2194$ and $A_e = 5.760$, $B_e = 0.3879$, $C_e = -0.2288$, $D_e = 0.1223$, $E_e = 1.8550$, and $F_e = 1780$ [14, 15]. As a first step in the development of the dispersion equations for ϵ -GaSe $_{1-x}$ S $_x$ ($x \leq 0.4$), identity of the point group symmetry for ϵ -GaSe and β -GaS crystals was considered in spite of their different polytypes. Then the dispersion properties of the ϵ -GaSe $_{0.6}$ S $_{0.4}$ (see the crystal polytype in [7]) were estimated from expression (1) with the use of expression (2) and the known dispersion equations for β -GaS crystals [1] as

$$n_{0,e}^2 = A_{0,e}/\lambda^4 + B_{0,e}/\lambda^2 + C_{0,e} + D_{0,e}\lambda^2 + E_{0,e}\lambda^4 \quad (3)$$

with the coefficients $A_0 = -0.03485$, $B_0 = 0.6305$, $C_0 = 6.556$, $D_0 = -0.001304$, and $E_0 = -0.00000203$ and $A_e = -0.03544$, $B_e = 0.3355$, $C_e = 4.954$, $D_e = -0.0008844$, and $E_e = -0.00001115$. Using values of the refractive indices obtained, the PM diagrams for second harmonic generation in ϵ -GaSe $_{0.6}$ S $_{0.4}$ were calculated. As expected, the estimated PM angles did not coincide with the experimental data most likely because of different polytypes of the initial crystals and/or incorrect coefficients in expression (3). However, the difference was not so large due to the identical point group symmetry; it did not exceed a few degrees in the most part of the spectral range of phase matching.

Then we corrected values of the refractive index for the GaSe $_{0.6}$ S $_{0.4}$ NSSC till coincidence of the estimated and experimental results. In so doing, we considered the following circumstances. The characteristic structural unit of the GaSe crystals having 4-atomic layered structure is a tetrahedral pyramid. The basis of the pyramid is an equilateral triangle with Se atoms in the vertices and the Ga atom in the vertex of the pyramid. The vertices of two such pyramids are oriented toward each other. The pyramids are bonded by their vertices, that is, by the Ga–Ga bond. The optical crystal axis is orthogonal to the pyramid bases. When the selenium atom is substituted by the sulfur atom with smaller dimensions during NSSC growth, the pyramid basis is deformed; it decreases thereby increasing the strength of bonds in the basal plane and the n_o value. The pyramid height decreases, and the strength of bonds in the direction of the optical axis increases to a lesser degree than in the basal plane [16] causing a smaller change of the n_e value. With allowance for this fact and small difference between experimentally measured and calculated matching angles, the dispersion dependence of n_e for the GaSe $_{0.6}$ S $_{0.4}$ NSSC was accepted as a true one. The dispersion dependence for n_o was corrected by the iterative method to make the estimated and experimental PM angles coincident with a preset accuracy of about 0.1°. Then the dispersion relations for the refractive indices n_o and n_e of the GaSe $_{0.6}$ S $_{0.4}$ crystal were approximated by equations

$$n_o^2 = 0.0231132/\lambda^4 + 0.325664/\lambda^2 + 7.11847 - 0.00247170\lambda^2 + 6.88091 \cdot 10^{-7}\lambda^4, \quad (4a)$$

$$n_e^2 = -0.0304705/\lambda^4 + 0.315179/\lambda^2 + 5.43810 - 0.00106289\lambda^2 - 4.50544 \cdot 10^{-6}\lambda^4. \quad (4b)$$

Based on Eqs. (2) that describe adequately the dispersion properties of the ϵ -GaSe crystals and Eqs. (4) derived for the GaSe $_{0.6}$ S $_{0.4}$ NSSC, dispersion equations (3) for the β -GaS crystals were also corrected; this was understood as a reassessment of the dispersion properties of the β -GaS crystals into the dispersion properties of the virtual ϵ -GaS crystal. In the process of growth of the ϵ -GaSe $_{1-x}$ S $_x$ NSSC, the structure of the β -GaS crystal was transformed into the structure of the ϵ -GaSe crystal with close structural parameters changing mostly insignificantly its dispersion properties. Calculated values of the refractive indices of the virtual ϵ -GaS crystal were approximated by the dispersion equations of the form

$$n_o^2 = 0.0211305/\lambda^4 + 0.206623/\lambda^2 + 6.62346 - 0.0040586\lambda^2 + 2.84447 \cdot 10^{-6}\lambda^4, \quad (5a)$$

$$n_e^2 = 0.0734480/\lambda^4 + 0.262196/\lambda^2 + 4.94284 - 0.00102111\lambda^2 - 1.07464 \cdot 10^{-5}\lambda^4. \quad (5b)$$

The PM angles for second harmonic generation in the $\text{GaSe}_{1-x}\text{S}_x$ ($0 < x < 0.4$) NSSC estimated using the expression [4]

$$n_e^2[\text{GaSe}_{1-x}\text{S}_x, 0 < x < 0.4] = (1-x) \cdot n_{oe}^2[\text{GaSe}] + x \cdot n_{oe}^2[\text{GaS}] \quad (6)$$

and Eq. (5) agreed with the experimental data to within 0.1° . Thus, Eq. (6) can be used in practice of designing frequency converters in the mid-IR range.

The adequacy of Eqs. (6) used to describe frequency conversion into the terahertz (THz) range of the spectrum was checked using a home-made difference-frequency generator for two generation lines of the TEA CO_2 laser operating at 10.3 and 10.6 μm . The TEA CO_2 laser generated single pulses with energy of 0.6–0.8 J in 150 ns leading peak. Pulse “tail” contained nearly 40% of the total pulse energy. To generate THz radiation by type II (oe \rightarrow e) interaction, two crystals with input apertures of $\varnothing 20$ mm were used: the pure GaSe crystal 14 mm long and the $\text{GaSe}_{0.8}\text{S}_{0.2}$ NSSC 16 mm long. The angle φ for type II THz emission was chosen after its preliminary identification from the experiment on type I second harmonic generation of the TEA CO_2 laser. Terahertz radiation with wavelength of 363.9 μm and energy per pulse of ~ 3 μJ was detected with an ELTEC 420M3 pyroelectric detector (France) for the pure GaSe crystal and the phase matching angle $\theta = 10.9^\circ$. A set of chosen organic filters was used to cut off pumping radiation. This result coincides within the limits of the measurement error with estimations from the data on the dispersion properties of the GaSe crystal presented in [14] and with the experimental results presented in [17]. Generation of THz radiation in the $\text{GaSe}_{0.8}\text{S}_{0.2}$ NSSC was excited for the matching angle smaller by 0.6° than that of the pure GaSe crystal.

CONCLUSIONS

It has been established that the short-wavelength absorption shoulder observed for some $\text{GaSe}_{1-x}\text{S}_x$ ($0 < x < 0.4$) NSSC samples is caused by the presence of spherical inclusions of metal gallium of micron and submicron sizes. This is in good agreement with the increased gallium content in these crystals in comparison with the initial charge content. This also suggests that the absorption peaks around 11.25 μm are caused by the presence of some other gallium and selenium compounds due to the excess of the gallium content and deficient sulfur content in comparison with the nominal charge content. The terahertz transmission spectrum of the $\text{GaSe}_{1-x}\text{S}_x$ NSSC is more attractive for down-conversion of IR-laser radiation compared to the transmission spectrum of the pure GaSe crystals. The suggested algorithm allows the dispersion equations to be developed for the $\text{GaSe}_{1-x}\text{S}_x$ ($x \leq 0.4$) NSSC in the form of a continuous function of the mixing ratio x . These equations are suitable for estimating the phase matching angles for second harmonic generation in mid-IR to within 0.1° .

This work was supported in part by the Russian Foundation for Basic Research (grants No. 07-02-92001-NNS_a and NSCT No. 96WFA0600007) and the Foundation for Promotion of the Russian Science.

REFERENCES

1. K. R. Allahverdiev, R. I. Guliev, T. Yu. Salaev, and V. V. Smirnov, *Kvant. Elektron.*, **9**, No. 7, 1483–1485 (1982).
2. S. Das, C. Ghosh, O. G. Voevodina, *et al.*, *Appl. Phys.*, **B81**, No. 8, 43–46 (2005).
3. V. G. Voevodin, S. A. Bereznaya, Z. V. Korotchenko, *et al.*, *Mater. Res. Soc. Symp. Proc.*, **829**, 375–382 (2005).
4. A. A. Tikhomirov, Yu. M. Andreev, G. V. Lanskii, *et al.*, *Proc. SPIE*, **6258**, 64–72 (2006).
5. Yu. M. Andreev, V. V. Atuchin, G. V. Lanskii, *et al.*, *Mater. Sci. Eng.*, **B128**, 205–210 (2006).
6. T.-J. Wang, J.-C. Gao, Yu. M. Andreev, *et al.*, *Russ. Phys. J.*, No. 6, 560–565 (2007).
7. H.-Z. Zhang, Z.-H. Kang, Y. Jiang, *et al.*, *Opt. Express*, **16**, 9951–9957 (2008).
8. P. Schunemann, *Laser Focus World*, No. 4, 85–90 (1999).

9. K. R. Allakhverdiev, T. Baykara, A. Kulibekov Gulubayov, *et al.*, *J. Appl. Phys.*, **98**, 093515 (1–6) (2005).
10. T. A. McMath and J. C. Irwin, *Phys. Status Solidi*, **38**, 731–737 (1976).
11. D. Errandonea, A. Segura, V. Munoz, and A. Chevy, *Phys. Rev.*, **B60**, 15866–15874 (1999).
12. M. Schluter, J. Camassel, S. Kohn, *et al.*, *Phys. Rev.*, **B13**, 3534–3547 (1976).
13. E. Takaoka and K. Kato, *Jpn. J. Appl. Phys.*, **38**, 2755–2759 (1999).
14. K. L. Vodopyanov and L. A. Kulevskii, *Opt. Commun.*, **118**, 375–378 (1995).
15. V. G. Dmitriev, G. G. Gurzadyan, and D. N. Nikogosyan, *Handbook of Nonlinear Optical Crystals*, Springer Verlag, New York; Berlin; Heidelberg (1997).
16. C. C. Wu, C. H. Ho, W. T. Shen, *et al.*, *Mater. Chem. Phys.*, **88**, 313–317 (2004).
17. S. Ya. Tochitsky, C. Sung, S. E. Trubnick, *et al.*, *J. Opt. Soc. Am.*, **B24**, 2509–2516 (2007).